Int. J. Environ. Sci. Technol. (2018) 15:1843–1850
https://doi.org/10.1007/s13762-017-1543-4

ORIGINAL PAPER

Non-destructive, high-resolution X-ray micro-CT of a Hairy Stalagmite: investigating the structural details of a biogenic speleothem

G. du Preez[1] · A. du Plessis[2,3] · D. de Beer[4] · P. Forti[5]

Received: 29 March 2017 / Revised: 7 August 2017 / Accepted: 10 September 2017 / Published online: 3 October 2017

Abstract Three-dimensional X-ray micro-computed tomography permits to investigate the internal structure of objects at a high resolution without altering its original form. It also facilitates the rendering and visualization of a virtual replica, which can be subjected to rigorous and complex analyses. In the present study, micro-computed tomography was used to investigate a unique and fragile speleothem (cave formation) named a "Hairy Stalagmite". Non-destructive analyses have revealed the calcareous internal structure of this speleothem, which consists of hollow, interconnected tubes. Rendered two-dimensional cross-sections also clearly revealed the outline of a once dense root nest that formed part of the speleothem's biogenic origin. The internal structure was further visualized using an image sequence of two-dimensional cross-sections to create a video that "brings the speleothem to life", also illustrating its complexity and variability. Statistical analyses revealed structural variability in void fraction, which is likely related to changing environmental conditions. In addition, the micro-computed tomography data were used as input for additive manufacturing (three-dimensional printing) in order to produce an enlarged replica of the Hairy Stalagmite sample, which made physical inspection possible. This combined approach represents the first of its kind and provides much benefit for future studies.

Keywords Additive manufacturing · Calcite tubes · Cave formations · Virtual replica

Editorial responsibility: Agnieszka Galuszka.

Electronic supplementary material The online version of this article (doi:10.1007/s13762-017-1543-4) contains supplementary material, which is available to authorized users.

✉ G. du Preez
speleo.africa@gmail.com

[1] Unit for Environmental Sciences and Management, North-West University, Potchefstroom, South Africa

[2] CT Scanner Facility, Stellenbosch University, Stellenbosch, South Africa

[3] Physics Department, Stellenbosch University, Stellenbosch, South Africa

[4] Technology Transfer and Innovation Support Office, North-West University, Potchefstroom, South Africa

[5] Italian Institute of Speleology, University of Bologna, Bologna, Italy

Introduction

In 2008, a new and rare biogenic root speleothem was discovered in a previously sealed cave of Botswana (Du Preez et al. 2015). This speleothem was named a "Hairy Stalagmite" and includes a nest of fine, living roots associated with the growing point (top) of the structure. This "root nest" captures and absorbs water from the cave necessary for the survival of Namaqua fig (*Ficus cordata*) trees in the Kalahari Desert (Du Preez et al. 2015). According to Du Preez et al. (2015), the Hairy Stalagmites are known from Dimapo and Diviner's Caves, which were both discovered and opened using geophysical and drilling techniques, respectively. These underground systems form part of the Gcwihaba Cave series located in Ngamiland, north-western Botswana.

The development of Hairy Stalagmites is uniquely linked and completely dependent on the presence of fig tree roots (Du Preez et al. 2015). The latter authors used stereo- and scanning electron microscopy (SEM) to provide evidence of the speleothem's fragility and biogenic origin,

which involves encrusting individual roots with a layer of calcite ($CaCO_3$). However, due to its organic nature, the root system itself either calcifies or decomposes over time, giving rise to a complex network of hollow and interconnected calcite tubes (Fig. 1). Although Du Preez et al. (2015) were able to discuss the developmental mechanism of this speleothem in detail, information relating to its internal structure remained limited since conventional 2D-sectioning is not only challenging and time consuming, but also destructive. Fortunately, modern technological advances, such as the application of three-dimensional (3D) X-ray micro-computed tomography (micro-CT), facilitate the in-depth study of objects in a reasonable amount of time without compromising its structural integrity.

X-ray CT (not to be confused with micro-CT) has previously been used to study the structure of larger speleothems (ranging between 20 cm and 36 cm in length), which generally presented high densities with variation in internal porosity (Mickler et al. 2004; Konečný et al. 2015; Walczak et al. 2015). Furthermore, a combination of X-ray CT and magnetic resonance imaging (MRI) has been used to study fluid inclusions, trapped within pores of calcite deposits (Zisu et al. 2012; Shtober-Zisu et al. 2014). Although computed tomography has been rarely applied in the study of speleothems (Vanghi et al. 2015), it presents great potential.

A more advanced approach is X-ray micro-CT, which has the added benefit of non-destructively studying the structural details of smaller objects at a high resolution (Du Plessis et al. 2016). Furthermore, with the additional application of virtual 3D rendering and visualization, different analyses can be undertaken and include determining feature directionality and connectivity, volumetric measurements, and advanced dimensional analysis of hidden internal features. Recent reviews on the application of this approach in geosciences (Cnudde and Boone 2013), food sciences (Schoeman et al. 2016), and material sciences (Maire and Withers 2014) are available for further reading. Micro-CT can also be used in conjunction with additive manufacturing (AM), also known as 3D-printing, to produce physical 3D replicas of the original objects (Du Plessis et al. 2014). However, although the advantages of AM are increasingly used in various fields of science, e.g. medicine (Booysen et al. 2011) and engineering (Krakhmalev et al. 2016), a literature study revealed no evidence of it ever being used to visually study the structure of a speleothem. Replicas of speleothems have, however, previously been created using moulds (Baeza and Durán 2015).

As a result of the clear benefits that X-ray micro-CT and AM provide, we decided to further investigate the internal structure of a Hairy Stalagmite using these techniques. This study was thus aimed at creating a high-quality, virtual replica of the original Hairy Stalagmite and subjecting it to an array of non-destructive analyses. Furthermore, a physical replica was also manufactured, which allowed visual inspection. This paper is the first to report on the utilization of advanced visualization and AM tools to produce 3D virtual and physical replicas of a speleothem, which serves as an example of how modern technological advances can help us gain insight into the structural details of nature's unique and fragile creations.

Sampling in Dimapo Cave (Ngamiland, north-western Botswana) occurred during September 2013. The analysis of this speleothem was commenced in 2016 at Stellenbosch University (South Africa).

Materials and methods

Micro-computed tomography scan

A dead Hairy Stalagmite (i.e. no living roots) sample was collected from Dimapo as described by Du Preez et al. (2015). The sample, sizing 86 mm in length with an average diameter of 20 mm, was subjected to micro-CT scans at the Stellenbosch University (South Africa) CT Scanner using a General Electric VTomex L240 system. Scans reported here were undertaken at the highest possible isotropic voxel resolution (18.6 μm) for this specific sample size. Sample preparation and scanning procedures were based on ASTM standards (ASTM 2011) and executed as

Fig. 1 A photograph of a dead Hairy Stalagmite sample collected from Dimapo Cave (Ngamiland, Botswana)

follows: the sample was mounted in a vertical position after which multiple scans were performed along the longitudinal axis. Basic scan settings were as follows: X-ray voltage = 150 kV, current = 100 μA, and duration = 250 ms per image acquisition. A full 360-degree rotation was successfully completed in 2400 steps (0.15° per step) with a total scan time of 180 min. At each step, the first image was discarded in order to minimize movement blur, while the subsequent two images were averaged to provide a higher signal-to-noise ratio. Furthermore, with detector sensitivity set to maximum, detector shift was activated to minimize ring artefacts, which are sometimes present as artificial rings in the top view of CT slice images. Reconstruction and stitching of the seven-part multiscan was achieved using Datos|× 2.0 software package (GE Measurement and Control, Germany). A multiscan involves scanning subsections of the studied object to obtain a higher resolution. In this case, the elongated shape of the speleothem required seven subsection scans, which were subsequently stitched together into one large volume (22 Gb).

Image processing

Image processing was completed using VGStudioMax 2.2 software package (Volume Graphics, Germany) by applying an advanced surface determination function to identify the internal edge between material (calcite structure) and void (both within the calcite tubes and that surrounding it). This process is similar to thresholding, however, it includes local optimization. This segmentation process was demonstrated in supplementary material. It is important to note that the interest was to visualize the larger pore spaces (network of tubes) and although some micro-porosity within white calcite-rich areas might have remained, this is not relevant to the present study. The white colour indicates denser material, with calcified material expected to be the densest material in the speleothem. Less dense material (e.g. any remaining organic material) was thus visualized as void (black in colour). Once the internal edge was identified, a combination of opening and closing morphological operations was applied to determine the external edge of the virtual sample. By doing so, all further analyses could be applied to only the internal structure of the virtual sample (thus excluding the space surrounding it). It should be noted that none of the image processing steps modified the data in any way; the executed steps allowed different selections to be made for visualization and analysis purposes only. Visualization (of a virtual Hairy Stalagmite replica) was accomplished through standard 2D contrasting and 3D thresholding operations.

Applied analyses

The performed analyses included (1) volumetric assessment of material and void, (2) defect analysis (assessment of the volume of each unconnected and separated internal pore), (3) fibre orientation analysis (directionality analysis of the selected component), and (4) wall thickness analysis (measurement of the thickness distribution of the cavities and calcite tube walls). Relative volumetric measurements were applied on well-defined regions as described in the segmentation step, i.e. selecting the edge between material and void in the 3D data set. Similar to 2D image analysis, thresholding was applied, however, with an additional localized refinement, which improves the final result compared to a global threshold. Void fraction data were plotted, tested for normality, and subjected to a nonparametric Spearman's correlation analysis using GraphPad Prism 6 software package (https://www.graphpad.com/scientific-software/prism). A Kruskal–Wallis analysis of variance (ANOVA) by ranks and multiple comparisons tests were performed using Statistica software package (http://www.statsoft.com). Effect sizes were calculated following Ellis and Steyn (2003).

The Volume Graphics fibre orientation analysis module was used to study the directionality of the calcite tubes. Using the reference orientation mode, the algorithm was applied on the air fraction of the speleothem sample. This was accomplished by using the advanced surface determination function and inverting the selected calcite region of interest. Furthermore, a wall thickness analysis module was executed and applied to the full 3D data set by selecting a maximum thickness of 1 mm and searching in a 30° angle.

3D-printing

The physical replica of the speleothem was created by selective laser sintering using polyamide PA2200 material. This was undertaken at the Vaal University of Technology's (South Africa) additive manufacturing facilities.

Results and discussion

After subjecting the Hairy Stalagmite sample (Fig. 1) to the above-described micro-CT and visualization procedures, a 3D virtual replica (Fig. 2a) was produced of which a 10-mm subsection (axial view) was enlarged (Fig. 2b). Furthermore, the internal structure of the entire speleothem sample was, for the first time, visualized as a virtual cross-section along the longitudinal axis (Fig. 3). As can be expected, what remains of the growing point (root nest) takes the form of a receptacle (cup) that traps water. From

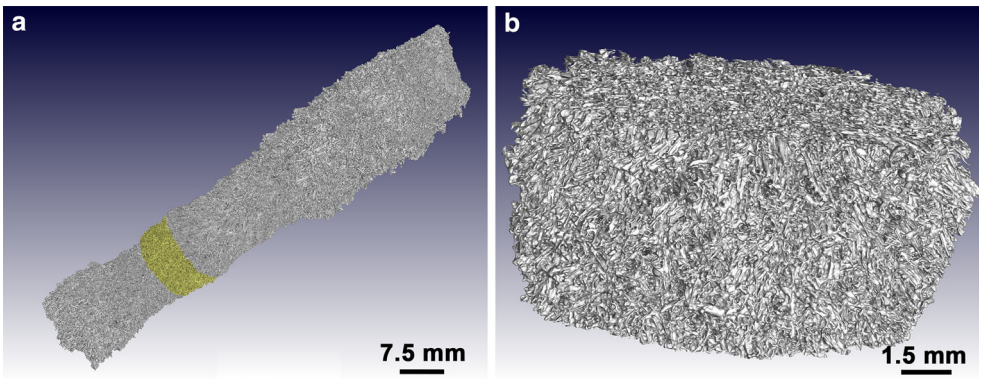

Fig. 2 Three-dimensional micro-computed tomography visualized image of a Hairy Stalagmite (**a**) with the yellow region indicating a selected area for close-up view (**b**)

Fig. 3, it is also evident that the structure is heterogenous with varying void fraction (internal porosity), diameter, and external features. Evidently, the internal structure of a Hairy Stalagmite is complex, which is consistent with the original findings of Du Preez et al. (2015).

Two axial cross-sections of low-porosity (Fig. 4a) and high-porosity (Fig. 4b) regions were also compared, which revealed structural differences. The low-porosity cross-section presents greater structural stability as calcite deposition is more evenly distributed and extends further inwards. On the contrary, the high-porosity cross-section clearly presents a larger void fraction with only the outer edges appearing to be substantially calcified. According to Du Preez et al. (2015), the visibly weaker calcified core is the result of constant introduction of water (from drips) during this stage of development, which inhibits supersaturation of $CaCO_3$ and thus calcite deposition. Other contributing factors may include (1) the droplet size and travel distance (kinetic energy), which can influence the outwards travel distance upon impact and (2) varying levels of root nest density. However, deviations from this general structural design (i.e. high-porosity core and calcified outer edge) were also discovered (Fig. 4c, d). Such examples include the lack of a visible core region (Fig. 4c) and increased calcite deposition in only one region of the cross-section (Fig. 4d). While the former might be the result of less frequent water drips during dry periods, the cause for the latter structural deviation remains unknown.

Also clearly visible are the comparatively larger (and somewhat circular) voids (Figs. 4 a, b) that likely represent the remnants of the decayed core root system from which smaller, lateral roots diverged (Du Preez et al. 2015). According to Du Preez et al. (2015), the larger roots are predominantly associated with the core of the speleothem likely as a result of it being the weakest part of the structure. As mentioned previously, calcite deposition is inhibited, while the impact of the water drops breaks apart already deposited calcite. On the contrary, the outer edge of the speleothem is subjected to high calcite deposition rates as a result of evaporation, CO_2 diffusion, and water uptake by roots. This also results in roots being encrusted with calcite before being able to substantially grow in size (Du Preez et al. 2015).

This intriguing root system was further visualized by creating a short (21 s) video clip (supplementary material) that consists of a sequence of 525 axial cross-section images. As this image sequence (of a 10-mm portion of the speleothem) plays from the base to the top, the root system itself "comes to life". The abundant fine roots are spread out across the speleothem and appear to extend in all directions. The larger roots, on the other hand, run

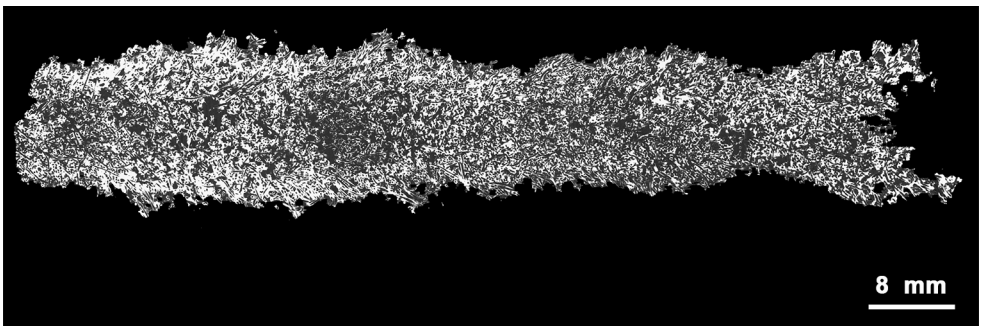

Fig. 3 Visualized micro-computed tomography slice image of a virtual cross-section in the longitudinal plane

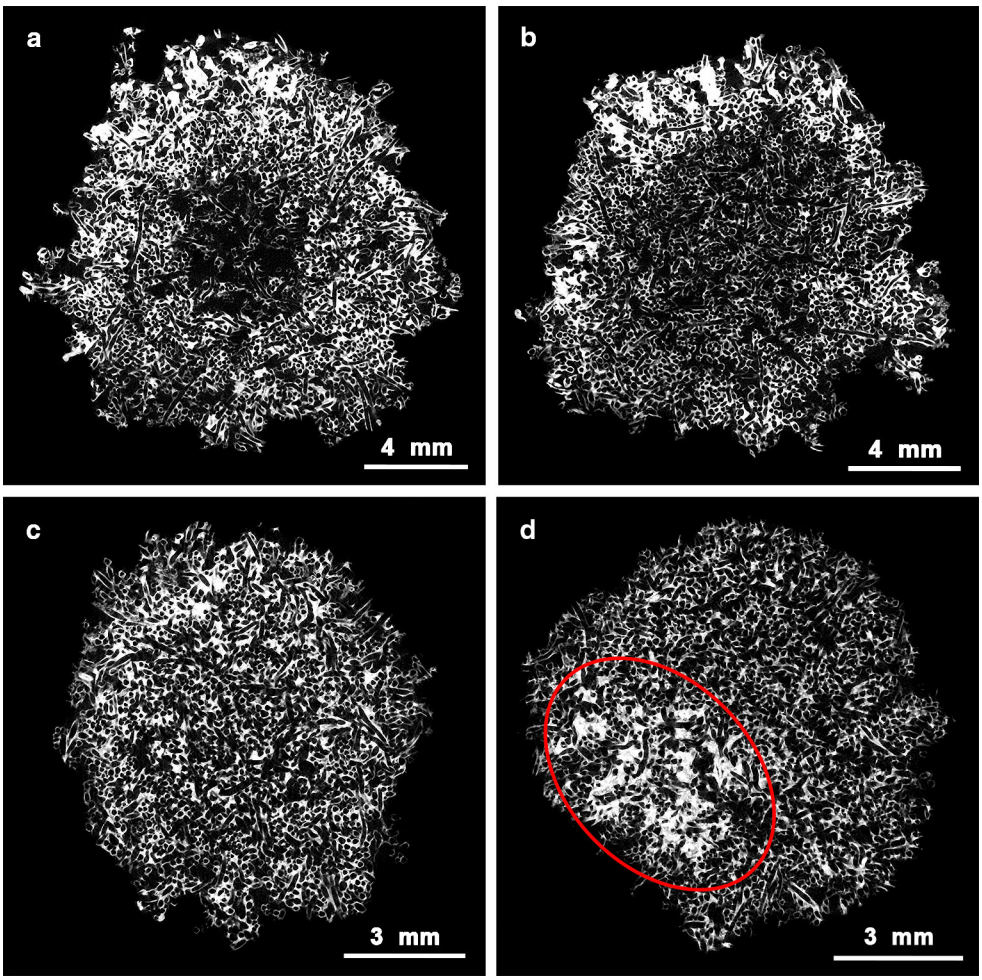

Fig. 4 Visualized micro-computed tomography axial cross-sections of low-porosity (**a**) and high-porosity (**b**) regions. Structural abnormalities were also detected as the lack of a visible core region (**c**) and increased calcite deposition (**d**) in only one specific region (encircled in red)

predominantly along the longitudinal axis with occasional diagonal or transverse extensions. As the image sequence approaches the top of the selected portion, it appears as if the core roots become more clustered.

However, the cross-sections and image sequence studied only specific regions of the Hairy Stalagmite sample. Subsequently, the total area, calcite area, and void area were calculated for each image stack and plotted on a xy diagram (Fig. 5). Although a nonparametric Spearman's correlation analysis revealed a significant ($p < 0.001$), positive correlation between calcite area and void area ($r = 0.81$), large deviations were still evident at 25 mm and 53 mm along the longitudinal axis. Furthermore, the void fraction percentage (Fig. 6) ranged from 15 to 40% along the longitudinal axis. Subsequently, six different subsections (Fig. 6) were selected for comparative analyses (Kruskal–Wallis ANOVA by ranks and multiple comparison tests), which showed that the means differed significantly ($p < 0.001$) with also significant ($p < 0.001$) differences between these subsections. Since these analyses

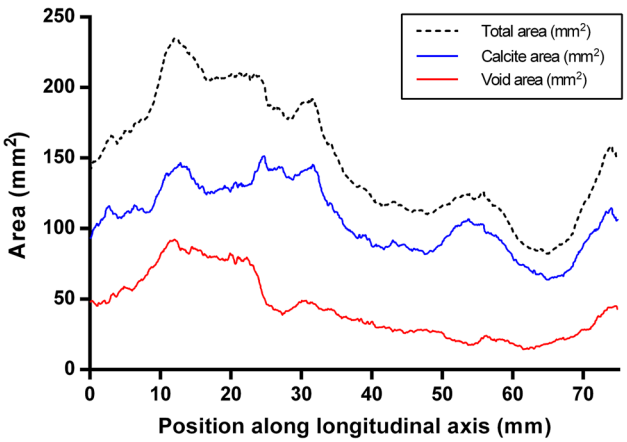

Fig. 5 Xy scatter plot of the total, calcite only, and void only areas of a Hairy Stalagmite sample as calculated from 2D micro-computed tomography slice images

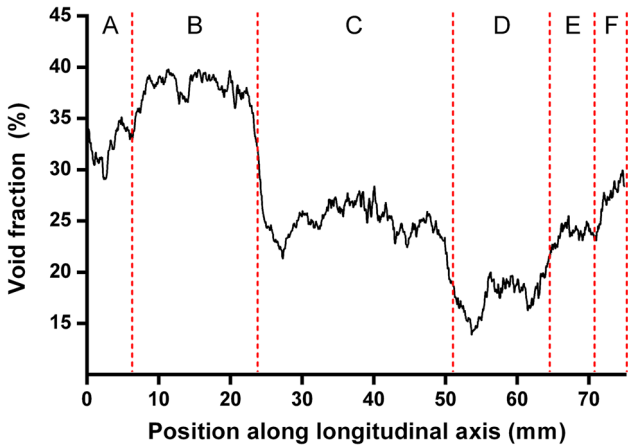

Fig. 6 Variation in void fraction percentage along the longitudinal axis of a Hairy Stalagmite sample. Red dotted lines indicate different sections of the sample that were subjected to further statistical analyses

were affected by sample size, it was decided to furthermore test for practical significance of differences or standardized differences (effect sizes). The results showed that all the subsections differed in practice (effect size >0.8) from one another. These findings suggest that variation in total surface area, visible as indentations (dents) on the outer surface of the speleothem, typically results in a related increase or decrease in both calcite area and void area. This and the observed variation in void area are likely the result of changing environmental factors (atmospheric conditions and water availability) and varying localized conditions (root nest density and water uptake) (Du Preez et al. 2015).

The directionality of the calcite tube (root) network was investigated by conducting a fibre orientation analysis ranging from the reference direction at 0° (vertical) to 90° (horizontal) (Fig. 7). This revealed that only a small portion (1.46%) of the calcite tubes developed near vertically (0°–9°), while a more even distribution of the calcite roots (67.24% of total) were angled between 45° and 90°. A recorded 13.99% of calcite tubes developed near horizontally (81°–90°). This is consistent with the finding of Du Preez et al. (2015), who studied 2D sections and revealed that some tubes developed radially from the centre of the stalagmite. Nevertheless, the fibre orientation analysis provided proof that although horizontal directionality might be favoured, the calcite roots developed in all of the studied directions. The physical characteristics of the calcite tubes were further studied with a wall thickness analysis function. This was applied to the void spaces in order to calculate an average tube thickness. The average tube thickness, as a function of height along the longitudinal axis of the speleothem, mostly varied between 130 and 140 µm (±60 µm). The large deviation indicates substantial variation in tube thickness and shows the complexity of the structure. This was also evident in the cross-sections (Fig. 4a–d), as well as the video clip (supplementary material). Scanning electron microscopy images acquired by Du Preez et al. (2015) also illustrate the variation in calcite tube thickness.

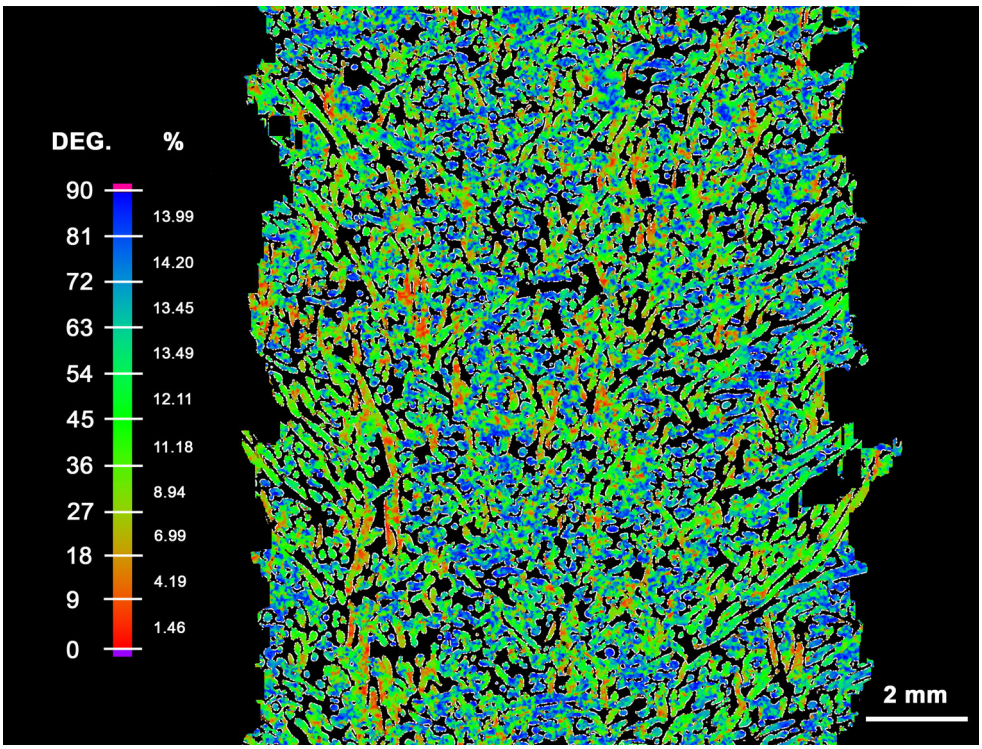

Fig. 7 Fibre orientation analysis illustrating the directionality of the calcite tubes. Each calcite tube (or tube section) was colour-coded according to its direction; for example, the reference directions at 0° (vertical) and 90° (horizontal) are represented by red and blue, respectively

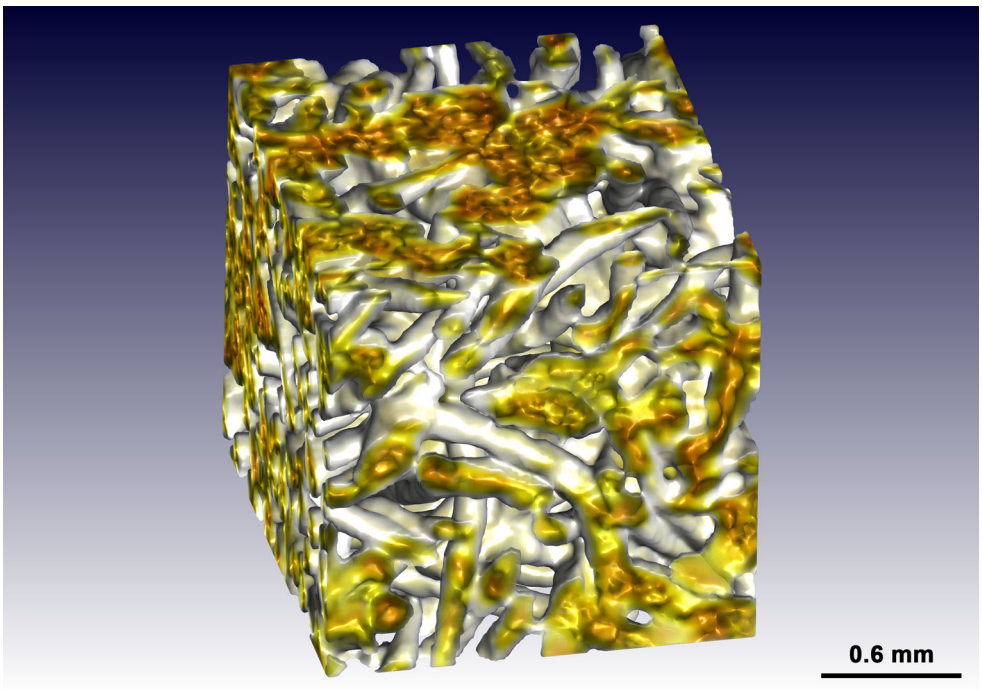

Fig. 8 Visualization of the original root network (now void) in a small section (2 × 2 × 2 mm) of a Hairy Stalagmite sample

Fig. 9 Physical replica of a Hairy Stalagmite sample created by additive manufacturing (3D-printing) for physical inspection

The void space was visualized in order to reanimate (illustrate) the original root network (Fig. 8), which more clearly indicated the morphology of the intertwined roots. Following, a physical replica of a portion of the scanned Hairy Stalagmite was manufactured (3D-printed) (Fig. 9). By printing the sample at 500% its original size, the speleothem could, for the first time, be physically inspected. Figure 9 clearly shows the complexity of its outer structure with various indentations and protrusions visible not only along the vertical axis, but across its entire surface.

Conclusion

For the first time, the technic of 3D X-ray micro-tomography was applied to an extraordinary complex and fragile speleothem: a "Hairy Stalagmite". This approach allowed for the visualization and physical inspection of the speleothem's microscopic structure with results supporting previous findings from 2D sectioning (Du Preez et al. 2015). It is therefore likely that 3D X-ray micro-tomography will become a commonly used analytic technic also in speleothem studies when morphological structures of second-order speleothems cannot be adequately studied using conventional methods.

Acknowledgements The authors thank Hannalene du Plessis and Suria Ellis for their valued statistical input.

References

ASTM (2011) E1570-11: Standard practice for computed tomographic (CT) examination. ASTM International. https://www.astm.org/Standards/E1570.htm. Accessed 1 Feb 2016

Baeza E, Durán J (2015) Proceso de realización de moldes y réplicas de un espeleotema singular: el caso de "La Palmatoria", Gruta de las Maravillas, Aracena (Huelva, España). Pesqu Tur Paisag Cársticas 8:65–73

Booysen G, Truscott M, Els J, De Beer D (2011) Development of patient-specific implants using direct metal laser sintering in titanium. In: Bártolo PJ, De Lemos ACS, Tojeira APO, Pereira AMH, Mateus AJ, Mendes ALA, Dos Santos C, Freitas DMF, Bártolo HM, Almeida HDA, Dos Reis IM, Dias JR, Domingos

MaN, Alves NMF, Pereira RFB, Patrício TMF, Ferreira TMD (eds) Proceedings of the 5th international conference on advanced research in virtual and rapid prototyping. CRC Press, Leiria, pp 145–153

Cnudde V, Boone MN (2013) High-resolution X-ray computed tomography in geosciences: a review of the current technology and applications. Earth Sci Rev 123:1–17

Du Plessis A, Seifert T, Booysen G, Els J (2014) Microfocus X-ray computed tomography (CT) analysis of laser sintered parts. S Afr J Ind Eng 25:39–49

Du Plessis A, Le Roux SG, Guelpa A (2016) The CT scanner facility at Stellenbosch University: an open access X-ray computed tomography laboratory. Nucl Instrum Method B 384:42–49

Du Preez GC, Forti P, Jacobs G, Jordaan A, Tiedt LR (2015) Hairy Stalagmites, a new biogenic root speleothem from Botswana. Int J Speleol 44:37–47

Ellis SM, Steyn HS (2003) Practical significance (effect sizes) versus or in combination with statistical significance (p-values). Manag Dyn J South Afr Inst Manag Sci 12:51–53

Konečný P, Lednická M, Souček K, Staš L, Kubina L, Gribovszki K (2015) Determination of dynamic Young's modulus of vulnerable speleothems. Acta Montan Slovaca 20:156–163

Krakhmalev P, Fredriksson G, Yadroitsava I, Kazantseva N, Du Plessis A, Yadroitsev I (2016) Deformation behavior and microstructure of Ti6Al4V manufactured by SLM. Phys Proc 83:778–788

Maire E, Withers P (2014) Quantitative X-ray tomography. Int Mater Rev 59:1–43

Mickler PJ, Ketcham RA, Colbert MW, Banner JL (2004) Application of high-resolution X-ray computed tomography in determining the suitability of speleothems for use in paleoclimatic, paleohydrologic reconstructions. J Cave Karst Stud 66:4–8

Schoeman L, Williams P, Du Plessis A, Manley M (2016) X-ray micro-computed tomography (μCT) for non-destructive characterisation of food microstructure. Trends Food Sci Technol 47:10–24

Shtober-Zisu N, Schwarcz HP, Chow T, Omelon CR, Southam G (2014) Caves in caves: evolution of post-depositional macroholes in stalagmites. Int J Speleol 43:323–334

Vanghi V, Iriarte E, Aranburu A (2015) High resolution X-ray computed tomography for petrological characterization of speleothems. J Cave Karst Stud 77:75–82

Walczak IW, Baldini JU, Baldini LM, McDermott F, Marsden S, Standish CD, Richards DA, Andreo B, Slater J (2015) Reconstructing high-resolution climate using CT scanning of unsectioned stalagmites: a case study identifying the mid-Holocene onset of the Mediterranean climate in southern Iberia. Quat Sci Rev 127:117–128

Zisu NS, Schwarcz HP, Konyer N, Chow T, Noseworthy MD (2012) Macroholes in stalagmites and the search for lost water. J Geophys Res 117:1–14